INTERNATIONAL JOURNAL FOR NUMERICAL AND ANALYTICAL METHODS IN GEOMECHANICS
Int. J. Numer. Anal. Meth. Geomech., 2004; **28**:1233–1255 (DOI: 10.1002/nag.385)

Stresses due to vertical subsurface loading for an inhomogeneous cross-anisotropic half-space

Cheng-Der Wang[1,*,†,‡] and Ernian Pan[2,§]

[1] *Department of Civil Engineering, National United University, Miao-Li, 360, Taiwan, R.O.C.*
[2] *Department of Civil Engineering, The University of Akron, Akron, U.S.A.*

SUMMARY

In this article, we present the solutions for the stresses induced by four different loads associated with an axially loaded pile in a continuously inhomogeneous cross-anisotropic half-space. The planes of cross-anisotropy are parallel to the horizontal surface of the half-space, and the Young's and shear moduli are assumed to vary exponentially with depth. The four loading types are: an embedded point load for an end-bearing pile, uniform skin friction, linear variation of skin friction, and non-linear parabolic variation of skin friction for a friction pile. The solutions for the stresses due to the pile load are expressed in terms of the Hankel integral and are obtained from the point load solutions of the same inhomogeneous cross-anisotropic half-space which were derived recently by the authors (*Int. J. Rock Mech. Min. Sci.* 2003; **40**(5):667–685). A numerical procedure is proposed to carry out the integral. For the special case of homogeneous isotropic and cross-anisotropic half-space, the stresses predicted by the numerical procedure agree well with the solutions of Geddes and Wang (*Geotechnique* 1966; **16**(3):231–255; *Soils Found.* 2003; **43**(5):41–52). An illustrative example is also given to investigate the effect of soil inhomogeneity, the type and degree of soil anisotropy, and the four different loading types on the vertical normal stress. The presented solutions are more realistic in simulating the actual stratum of loading problem in many areas of engineering practice. Copyright © 2004 John Wiley & Sons, Ltd.

KEY WORDS: stresses; inhomogeneous cross-anisotropic half-space; axially loaded pile; embedded point load; uniform skin friction; linear variation of skin friction; non-linear parabolic variation of skin friction

INTRODUCTION

In most previous theoretical analysis of soil behaviour, the properties of soil were assumed to be homogeneous and isotropic. However, many natural soils, such as flocculated clays, varved silts or sands, often deposited through a geologic process of sedimentation over a period of time. The effects of deposition, overburden, desiccation, etc., can lead geological media, which usually exhibit the anisotropic and inhomogeneous deformability. The mechanical response of anisotropic materials with spatial gradients in composition is of considerable interest in soil/rock mechanics [1]. In this work, an elastic loading problem for a continuously inhomogeneous cross-anisotropic half-space with Young's and shear moduli varying exponentially with depth is relevant.

*Correspondence to: Cheng-Der Wang, Department of Civil Engineering, National United University, 1 Lien-Da, Kung-Ching-Li, Miao-Li, 360, Taiwan, R.O.C.
† E-mail: cdwang@nuu.edu.tw
‡ Associate Professor
§ Associate Professor

Received 6 December 2003
Revised 21 March 2004

It is known that piles transmit axial loads to the ground by the mechanism of end-bearing or skin friction [2]. For an isotropic soil mass, the displacements and stresses can be obtained by using the Mindlin's solution [3] where a vertical point load is applied in the interior of the half-space. Grillo [4] presented the influence charts (Poisson's ratio = 0.5) for the vertical normal stress due to a pile point load, and uniform skin friction along the pile, respectively. However, his solutions contained a number of inconsistencies and errors that were later on pointed out by Geddes [5]. Geddes [5] obtained the analytical solution based on the Mindlin's solution [3] for the stresses at any point, over the length of the pile in a cylindrical co-ordinate system due to a point load, uniform skin friction, and linear variation of skin friction. He also prepared the most commonly used tables of stress coefficients for Poisson's ratio equal to 0.1, 0.3, and 0.5, respectively [5, 6]. However, these solutions are all restricted to the homogeneous and isotropic half-spaces. As for the homogeneous and cross-anisotropic half-space, Wang [7] recently derived the analytical solutions for the displacements and stresses due to various loading types of an axially loaded pile. Besides the three loading types studied by Geddes [5, 6], Wang [7] also gave the displacement and stress solutions due to the non-linear parabolic variation of skin friction for a friction pile. Yet, consideration of inhomogeneity of soils may be more realistic in many cases and may more accurately reflect the transfer of load from the pile to the soil [8]. So far, to the best of the authors' knowledge, however, no such solutions exist for the stresses due to the above-mentioned loading types in an inhomogeneous cross-anisotropic half-space say, with Young's and shear moduli varying exponentially with depth ($E\mathrm{e}^{-kz}, E'\mathrm{e}^{-kz}, G'\mathrm{e}^{-kz}$). The lack of such solutions is mainly due to the fact that the general method for solving the problem involving inhomogeneity and anisotropy is more complicated.

It is well recognized that the point load solution forms the basis of solutions to complex loading problems. Utilizing the approach for solving a point load problem by Liao and Wang [9], Wang *et al.* [10, as seen in Figure 1] derived the point load solution of stresses in the Hankel-transformed domain for a continuously inhomogeneous cross-anisotropic full and half-spaces subjected to a vertical point load. Numerical inversion of the Hankel transforms is needed to find the physical domain stresses since the resulting integrals in the point load solution involve products of Bessel functions of the first kind, an exponential function, and a polynomial, which cannot be given in the exact closed-form.

In this paper, we derive the semi-analytical solutions for stresses in an inhomogeneous and cross-anisotropic half-space induced by an end-bearing (a point load), and various skin frictions (uniform, linearly varying, and non-linearly parabolic varying) of an axially loaded pile. These solutions are obtained by integrating the point load solution derived by Wang *et al.* [10]. However, it should be noted that the proposed solutions are not for the pile-soil interactions. Rather, they are semi-coupled solutions where the influences of the pile on the soil foundation are simplified as various distributed loads. Also, the presented solutions are based on the assumptions that the medium is a linear elastic, and the cross-anisotropic half-space has planes of isotropy parallel to the boundary plane. Additionally, the effect of pile diameter is not considered in this analysis. Therefore, in this work, four cases of vertical loadings given below are considered:

Case A. A point load F (force), at depth L (Figure 2). This case is called point load.

Case B. A total load of Q (force per unit length), applied along the vertical axis z in uniform distribution ($Q(z) = F/L$) from the surface to depth L (Figure 3). This case is called uniform skin friction.

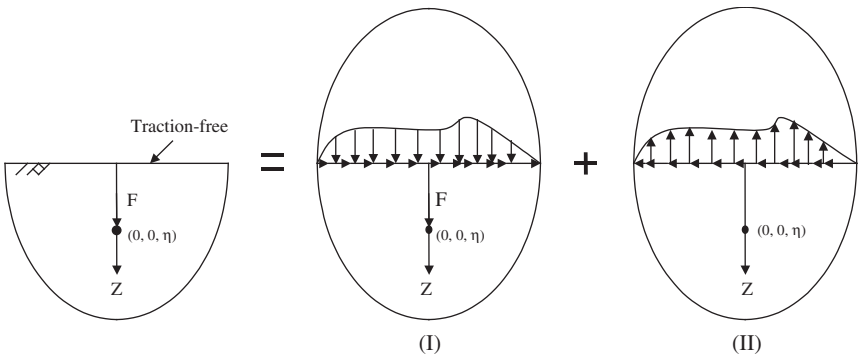

Figure 1. Superposition approach to the point loading half-space problem.

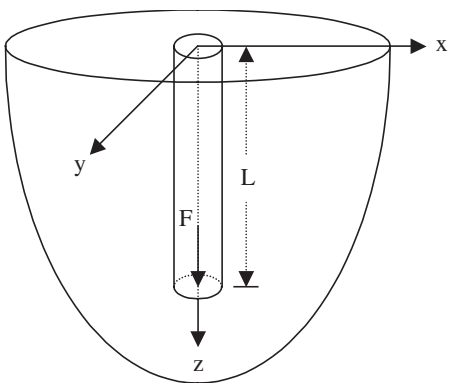

Figure 2. An inhomogeneous cross-anisotropic half-space subjected to a point load.

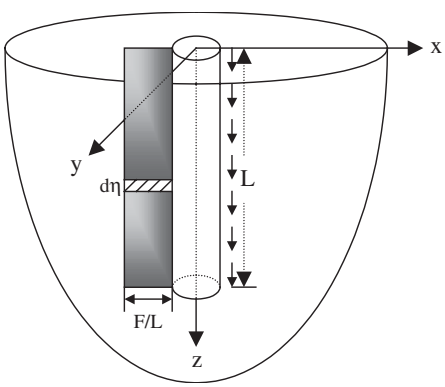

Figure 3. An inhomogeneous cross-anisotropic half-space subjected to a uniform skin friction.

Case C. A total load of Q (force per unit length), applied along the vertical axis z in increments varying linearly with depth ($Q(z) = (2F/L^2)z$), from zero at the surface to a maximum at depth L (Figure 4). This case is called linear variation of skin friction.

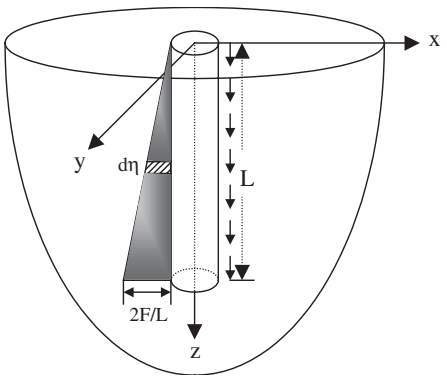

Figure 4. An inhomogeneous cross-anisotropic half-space subjected to a linear variation of skin friction.

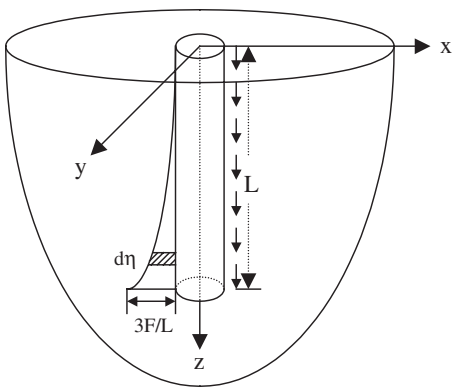

Figure 5. An inhomogeneous cross-anisotropic half-space subjected to a non-linear parabolic variation of skin friction.

Case D. A total load of Q (force per unit length), applied along the vertical axis z in increments varying non-linearly parabolic with depth ($Q(z) = (3F/L^3)z^2$), from zero at the surface to a maximum at depth L (Figure 5). This case is called non-linear parabolic variation of skin friction.

An illustrative example is given to demonstrate the influence of soil inhomogeneity, the type and degree of soil anisotropy, and the loading types on the vertical normal stress, which could be useful to the design of soil foundation and piles.

CASE A: STRESSES DUE TO A POINT LOAD

The approaches for solving the stresses subjected to a static point load F in a cylindrical co-ordinate, which are expressed as the form of body forces, are shown in Figure 1 [10]. Figure 1 depicts that a half-space is composed of two full-spaces, one with a point load in its interior and the other with opposite traction of the first full-space along $z = 0$. The traction in the first

full-space along $z = 0$ is due to the point load. The solutions for the half-space are thus obtained by superposing the solutions of the two full-spaces. That is, the solutions can be derived from the governing equations for a full-space (including the general solutions (I) and homogeneous solutions (II)) by satisfying the traction-free boundary conditions on the surface of the half-space. The Hankel transforms with respect to r are employed for solving this problem. Hence, the solutions in the Hankel-transformed domain for the vertical normal stress ($\sigma_{zz}^{p^*}$) and shear stress ($\tau_{rz}^{p^*}$) subjected to a point load F acting at $z = \eta$ (measured from the surface, as shown in Figure 1) in the interior of an inhomogeneous cross-anisotropic half-space are expressed as follows:

$$\sigma_{zz}^{p^*} = \frac{F}{4\pi C_{33}C_{44}}\left[A_1 e^{-u_1\xi|z-\eta|} + A_2 e^{(k-u_2\xi)|z-\eta|} - A_1\frac{\Delta_1}{\Delta}e^{-u_1\xi(z+\eta)} - A_3\frac{\Delta_2}{\Delta}e^{(k-u_1\xi)z}e^{-u_2\xi\eta} - A_4\frac{\Delta_3}{\Delta}e^{(k-u_2\xi)z}e^{-u_1\xi\eta} - A_2\frac{\Delta_4}{\Delta}e^{(k-u_2\xi)(z+\eta)}\right] \quad (1)$$

$$\tau_{rz}^{p^*} = \frac{-F}{4\pi C_{33}}\left[B_1 e^{-u_1\xi|z-\eta|} + B_2 e^{(k-u_2\xi)|z-\eta|} + B_1\frac{\Delta_1}{\Delta}e^{-u_1\xi(z+\eta)} + B_3\frac{\Delta_2}{\Delta}e^{(k-u_1\xi)z}e^{-u_2\xi\eta} + B_4\frac{\Delta_3}{\Delta}e^{(k-u_2\xi)z}e^{-u_1\xi\eta} + B_2\frac{\Delta_4}{\Delta}e^{(k-u_2\xi)(z+\eta)}\right] \quad (2)$$

where

$$A_1 = \frac{[(C_{33}C_{44}u_1^2 + C_{13}^2 + C_{13}C_{44} - C_{11}C_{33})u_1\xi^2 + kC_{44}(C_{33}u_1^2 + C_{13})\xi]}{u_1[(k + u_1\xi)^2 - u_2^2\xi^2]}$$

$$A_2 = \frac{[(C_{33}C_{44}u_2^2 + C_{13}^2 + C_{13}C_{44} - C_{11}C_{33})u_2\xi^2 - k(2C_{33}C_{44}u_2^2 + C_{13}^2 - C_{11}C_{33})\xi + k^2C_{33}C_{44}u_2]}{u_2[(k - u_2\xi)^2 - u_1^2\xi^2]}$$

$$A_3 = \frac{[(C_{33}C_{44}u_1^2 + C_{13}^2 + C_{13}C_{44} - C_{11}C_{33})u_1\xi^2 + k(C_{13}C_{44} + C_{11}C_{33})\xi - k^2C_{33}C_{44}u_1]}{u_2[(k - u_2\xi)^2 - u_1^2\xi^2]}$$

$$A_4 = \frac{[(C_{33}C_{44}u_2^2 + C_{13}^2 + C_{13}C_{44} - C_{11}C_{33})u_2\xi^2 - k(2C_{33}C_{44}u_2^2 + C_{13}^2 - C_{11}C_{33})\xi + k^2C_{33}C_{44}u_2]}{u_1[(k - u_1\xi)^2 - u_2^2\xi^2]}$$

$$\begin{aligned}\Delta = {} & \{C_{13}[(C_{13} + C_{44})u_1\xi + kC_{44}] + C_{33}u_1[(-C_{11} + C_{44}u_1^2)\xi + kC_{44}u_1]\} \\ & \times \{(k - u_2\xi)[(C_{13} + C_{44})u_2\xi - kC_{13}] + [(-C_{11} + C_{44}u_2^2)\xi^2 - kC_{44}u_2\xi]\} \\ & + \{u_1[(C_{13} + C_{44})u_1\xi + kC_{44}] - [(-C_{11} + C_{44}u_1^2)\xi + kC_{44}u_1]\} \\ & \times \{C_{13}[(C_{13} + C_{44})u_2\xi^2 - kC_{13}\xi] - C_{33}(k - u_2\xi)[(-C_{11} + C_{44}u_2^2)\xi - kC_{44}u_2]\}\end{aligned}$$

$$\begin{aligned}\Delta_1 = {} & \{C_{13}[(C_{13} + C_{44})u_1\xi + kC_{44}] - C_{33}u_1[(-C_{11} + C_{44}u_1^2)\xi + kC_{44}u_1]\} \\ & \times \{(k - u_2\xi)[(C_{13} + C_{44})u_2\xi - kC_{13}] + [(-C_{11} + C_{44}u_2^2)\xi^2 - kC_{44}u_2\xi]\} \\ & - \{u_1[(C_{13} + C_{44})u_1\xi + kC_{44}] + [(-C_{11} + C_{44}u_1^2)\xi + kC_{44}u_1]\} \\ & \times \{C_{13}[(C_{13} + C_{44})u_2\xi^2 - kC_{13}\xi] - C_{33}(k - u_2\xi)[(-C_{11} + C_{44}u_2^2)\xi - kC_{44}u_2]\}\end{aligned}$$

$$\Delta_2 = 2(k - u_2\xi)\{C_{13}[(C_{13} + C_{44})u_2\xi - kC_{13}]^2 + C_{33}[(-C_{11} + C_{44}u_2^2)\xi - kC_{44}u_2]^2\}$$

$$\Delta_3 = 2u_1\xi\{C_{13}[(C_{13}+C_{44})u_1\xi + kC_{44}]^2 + C_{33}[(-C_{11}+C_{44}u_1^2)\xi + kC_{44}u_1]^2\}$$

$$\begin{aligned}\Delta_4 = & -\{C_{13}[(C_{13}+C_{44})u_1\xi + kC_{44}] + C_{33}u_1[(-C_{11}+C_{44}u_1^2)\xi + kC_{44}u_1]\}\\ & \times\{(k-u_2\xi)[(C_{13}+C_{44})u_2\xi - kC_{13}] - [(-C_{11}+C_{44}u_2^2)\xi^2 - kC_{44}u_2\xi]\}\\ & +\{u_1[(C_{13}+C_{44})u_1\xi + kC_{44}] - [(-C_{11}+C_{44}u_1^2)\xi + kC_{44}u_1]\}\\ & \times\{C_{13}[(C_{13}+C_{44})u_2\xi^2 - kC_{13}\xi] + C_{33}(k-u_2\xi)[(-C_{11}+C_{44}u_2^2)\xi - kC_{44}u_2]\}\end{aligned}$$

$$B_1 = \frac{(C_{11}+C_{13}u_1^2)\xi^2}{u_1[(k+u_1\xi)^2 - u_2^2\xi^2]}$$

$$B_2 = \frac{[(C_{11}+C_{13}u_2^2)\xi^2 - 2kC_{13}u_2\xi + k^2C_{13}]}{u_2[(k-u_2\xi)^2 - u_1^2\xi^2]}$$

$$B_3 = \frac{[(C_{11}+C_{13}u_1^2)\xi^2 - k(C_{13}+C_{44})u_1\xi - k^2C_{13}]}{u_2[(k-u_2\xi)^2 - u_1^2\xi^2]}$$

$$B_4 = \frac{[(C_{11}+C_{13}u_2^2)\xi^2 - 2kC_{13}u_2\xi + k^2C_{13}]}{u_1[(k-u_1\xi)^2 - u_2^2\xi^2]}$$

In Equations (1)–(2), C_{ij} $(i,j = 1\text{–}6)$ are the elastic stiffness coefficients of a continuously inhomogeneous cross-anisotropic medium, which in a cylindrical co-ordinate system are given by:

$$\begin{bmatrix}\sigma_{rr}\\ \sigma_{\theta\theta}\\ \sigma_{zz}\\ \tau_{\theta z}\\ \tau_{rz}\\ \tau_{r\theta}\end{bmatrix} = \begin{bmatrix}C_{11} & C_{11}-2C_{66} & C_{13} & 0 & 0 & 0\\ C_{11}-2C_{66} & C_{11} & C_{13} & 0 & 0 & 0\\ C_{13} & C_{13} & C_{33} & 0 & 0 & 0\\ 0 & 0 & 0 & C_{44} & 0 & 0\\ 0 & 0 & 0 & 0 & C_{44} & 0\\ 0 & 0 & 0 & 0 & 0 & C_{66}\end{bmatrix}\begin{bmatrix}\varepsilon_{rr}\\ \varepsilon_{\theta\theta}\\ \varepsilon_{zz}\\ \gamma_{\theta z}\\ \gamma_{rz}\\ \gamma_{r\theta}\end{bmatrix} e^{-kz} \tag{3}$$

where k is referred to as the inhomogeneity parameter. Furthermore, we notice that C_{ij} can be expressed in terms of the five engineering elastic coefficients E, E', v, v' and G' as:

$$C_{11} = \frac{E(1-(E/E')v'^2)}{(1+v)(1-v-(2E/E')v'^2)}, \quad C_{13} = \frac{Ev'}{1-v-(2E/E')v'^2},$$
$$C_{33} = \frac{E'(1-v)}{1-v-(2E/E')v'^2}, \quad C_{44} = G', \quad C_{66} = \frac{E}{2(1+v)} \tag{4}$$

where

1. E and E' are Young's moduli in the plane of cross-anisotropy and in a direction normal to it, respectively.
2. v and v' are Poisson's ratios characterizing the lateral strain response in the plane of cross-anisotropy to a stress acting parallel and normal to it, respectively.
3. G' is the shear modulus in planes normal to the plane of cross-anisotropy.

However, u_1 and u_2 are two characteristic roots obtained based on the assumption on the elastic coefficients [10], and can be defined as:

$$u_1 = \sqrt{\frac{S + \sqrt{S^2 - 4Q}}{2}}, \quad u_2 = \sqrt{\frac{S - \sqrt{S^2 - 4Q}}{2}}$$

where

$$S = \frac{C_{11}C_{33} - C_{13}(C_{13} + 2C_{44})}{C_{33}C_{44}}, \quad Q = \frac{C_{11}}{C_{33}}$$

The differences between the homogeneous cross-anisotropic elastic coefficients [9] and the inhomogeneous ones [10] adopted in this paper are expressed in Table I. It is clear that, for an inhomogeneous cross-anisotropic half-space described by Equation (3), only three (E, E', and G') of the five engineering elastic coefficients depend exponentially on the inhomogeneity parameter k; the two Poisson's ratios are still constants. Besides, depending on the parameter k, we have the following three different situations:

(1) $k > 0$, denotes a hardened surface, whereas E, E', and G' decrease with the increase of depth.
(2) $k = 0$, is referred to as the conventional homogeneous case [9].
(3) $k < 0$, denotes a soft surface, whereas E, E', and G' increase with the increase of depth.

The stresses $\sigma_{zz}^{\mathrm{p}}, \tau_{rz}^{\mathrm{p}}$ in the physical domain for the inhomogeneous and cross-anisotropic half-space can be obtained by taking the inverse Hankel transform for $\sigma_{zz}^{\mathrm{p}*}$ (Equation (1)), $\tau_{rz}^{\mathrm{p}*}$ (Equation (2)) with respect to ξ of order 0, and 1, respectively, in the following:

$$\begin{Bmatrix} \sigma_{zz}^{\mathrm{p}} \\ \tau_{rz}^{\mathrm{p}} \end{Bmatrix} = \int_0^\infty \xi \begin{Bmatrix} \sigma_{zz}^{\mathrm{p}*} J_0(\xi r) \\ \tau_{rz}^{\mathrm{p}*} J_1(\xi r) \end{Bmatrix} \mathrm{d}\xi \tag{5}$$

From Equations (1)–(2), we found that the integrands under the infinite integrals in Equation (5) involve products of Bessel function of the first kind of order n ($n = 0, 1$), an exponential function, and a polynomial, which cannot be given in closed-form so that numerical integrations are required. The numerical methods employed are to perform the integration over each of the first 20 half-cycles of Bessel functions. Additionally, Euler's transformation was applied to this series to speed up the convergence [11]. The first twenty terms of zeros of Bessel function of the first kind of order n ($n = 0, 1$) are quoted from Watson [12]. Also, the Gauss quadrature formula was utilized for 68 points of subdivision of each interval in order to obtain high accuracy of numerical values. The method proposed by Longman [11] can be expressed as follows:

$$\int_0^\infty J_0(x)\,\mathrm{d}x \cong \sum_{n=0}^{20} \int_{x_n}^{x_{n+1}} J_0(x)\,\mathrm{d}x \tag{6}$$

Table I. Homogeneous and inhomogeneous cross-anisotropic elastic coefficients.

Homogeneous [9]	Inhomogeneous [10]
E	$E\mathrm{e}^{-kz}$
E'	$E'\mathrm{e}^{-kz}$
v	v
v'	v'
G'	$G'\mathrm{e}^{-kz}$

In each division, the 16 points of Gaussian quadrature are adopted, and x can be transferred by:

$$x = \frac{(x_{n+1} - x_n)t + x_{n+1} + x_n}{2} \tag{7}$$

with t being the Gauss point.

Then, revising Equation (6) with Equation (7) yields the following expression:

$$\sum_{n=0}^{20} \int_{x_n}^{x_{n+1}} J_0(x)\,\mathrm{d}x \cong \sum_{n=0}^{20} \frac{(x_{n+1} - x_n)}{2} \left[\sum_{i=1}^{16} w_i J_0 \left(\frac{(x_{n+1} - x_n)t_i + x_{n+1} + x_n}{2} \right) \right] \tag{8}$$

In order to accelerate the convergence, we sum up the values of the first 10 terms, and introduce the Euler's transformation to the other tens as:

$$\int_0^{\infty} J_0(x)\,\mathrm{d}x \cong \sum_{n=0}^{10} \int_{x_n}^{x_{n+1}} J_0(x)\,\mathrm{d}x + \sum_{n=11}^{20} \frac{\Lambda^{n-10}}{2^{n-10}} = 0.999999992 \tag{9}$$

where Λ is the first advancing row of the differences [11], and n is a constant ranging from 0 to 20. Thus, the approximate value (0.999999992) calculated by Equation (9) is very close to the exact result (which is equal to 1.0).

The singularities encountered can be solved by means of the Taylor's expansion theorem as [13]:

$$\begin{aligned} f(x) &= \int_a^b \frac{f(t)}{t-x}\,\mathrm{d}t = \int_a^b \frac{f(t)-f(x)}{t-x}\,\mathrm{d}t + \int_a^b \frac{f(x)}{t-x}\,\mathrm{d}t = \int_a^b \frac{f(t)-f(x)}{t-x}\,\mathrm{d}t + f(x)\log\frac{b-x}{x-a} \\ &= \int_a^{x-\varepsilon} \frac{f(t)-f(x)}{t-x}\,\mathrm{d}t + \int_{x-\varepsilon}^b \frac{f(t)-f(x)}{t-x}\,\mathrm{d}t + f(x)\log\frac{b-x}{x-a} + 2\varepsilon f'(x) + \frac{\varepsilon^3}{9} f'''(x) + \cdots \end{aligned} \tag{10}$$

where x is a singular point; a, b are the lower, upper limit, respectively; ε is a tiny parameter with respect to the integral interval $b - a$.

Thus, the stresses for an end-bearing pile in the inhomogeneous and cross-anisotropic half-space, as seen in Figure 2, can be obtained by substituting η by L in Equation (5). The numerical results are in good agreement with the Mindlin's [3] and Geddes's solutions [5] when the medium is homogeneous and isotropic (as seen in Figure 6 in the illustrative examples section), and with Wang's solutions [7] when the medium is homogeneous but cross-anisotropic (as seen in Figures 7–9 in the Illustrative Examples section).

CASE B: STRESSES DUE TO A UNIFORM SKIN FRICTION

The stresses in an inhomogeneous and cross-anisotropic half-space due to a uniform skin friction can be directly integrated from the point load solutions. The total load Q (force per unit length) is distributed uniformly with depth from the surface at $z = 0$ to the depth at $z = L$ (Figure 3). Taking an infinitesimal element $\mathrm{d}\eta$ along the z-axis, the elementary force can be expressed as follows:

$$\mathrm{d}Q = \left(\frac{F}{L}\right)\mathrm{d}\eta \tag{11}$$

Hence, integrating η in Equations (1)–(2) between the limits 0 and L gives:

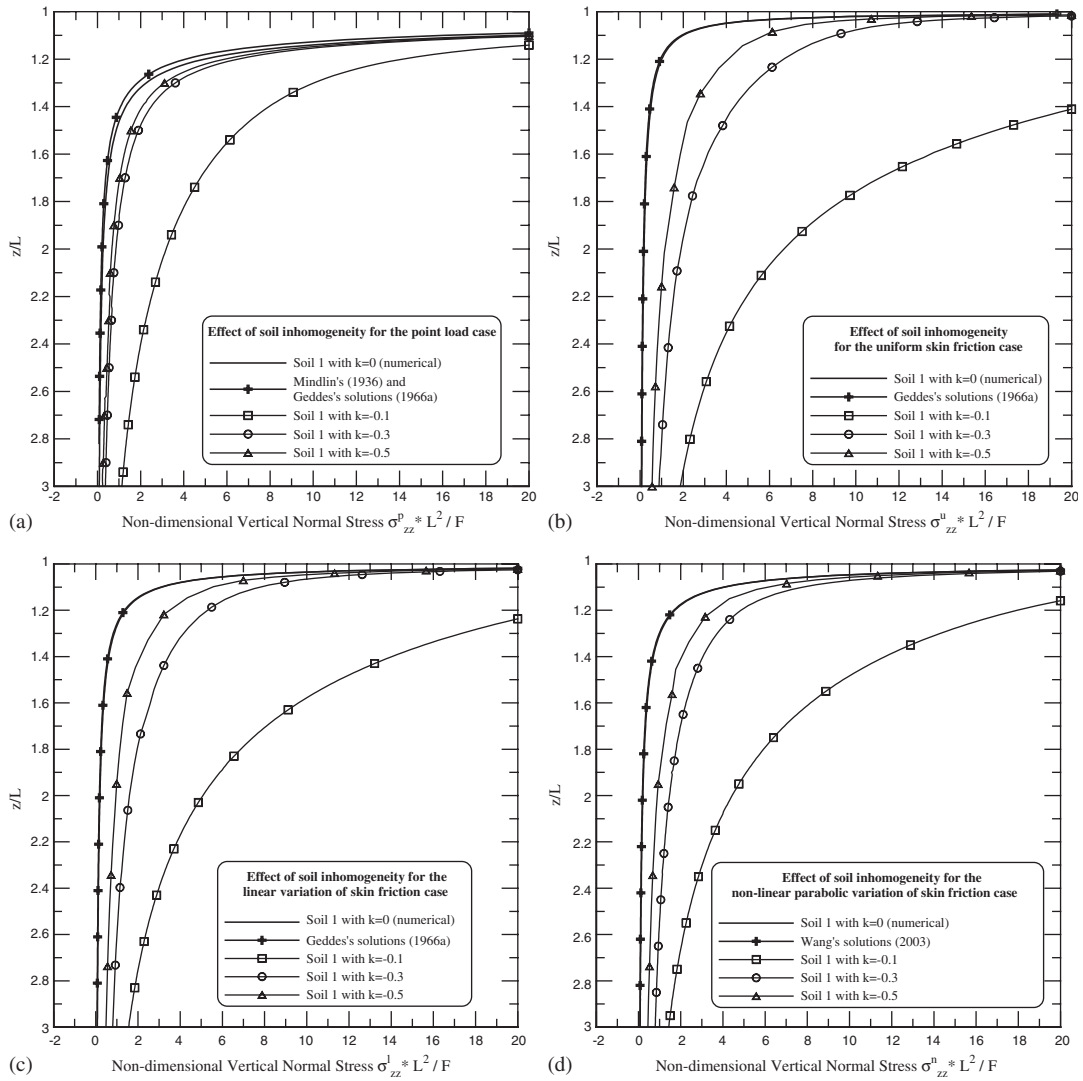

Figure 6. Effect of soil inhomogeneity. Variation of non-dimensional vertical normal stress with non-dimensional depth below the loading line in inhomogeneous Soil 1: Point load in (a); uniform skin friction in (b); linear variation of skin friction in (c); and non-linear parabolic variation of skin friction in (d).

$$\sigma^{u*}_{zz} = \frac{F}{4\pi C_{33} C_{44} L}\left\{ -A_1 \frac{1}{u_1 \xi}[e^{-u_1\xi z} - e^{-u_1\xi(z-L)}] + A_2 \frac{1}{(k-u_2\xi)}[e^{(k-u_2\xi)z} - e^{(k-u_2\xi)(z-L)}] \right.$$
$$- A_1 \frac{\Delta_1}{\Delta}\frac{1}{u_1\xi}[e^{-u_1\xi z} - e^{-u_1\xi(z+L)}] - A_3 \frac{\Delta_2}{\Delta}\frac{1}{u_2\xi}(1 - e^{-u_2\xi L})e^{(k-u_1\xi)z}$$
$$\left. -A_4 \frac{\Delta_3}{\Delta}\frac{1}{u_1\xi}(1 - e^{-u_1\xi L})e^{(k-u_2\xi)z} + A_2 \frac{\Delta_4}{\Delta}\frac{1}{(k-u_2\xi)}[e^{(k-u_2\xi)z} - e^{(k-u_2\xi)(z+L)}] \right\} \quad (12)$$

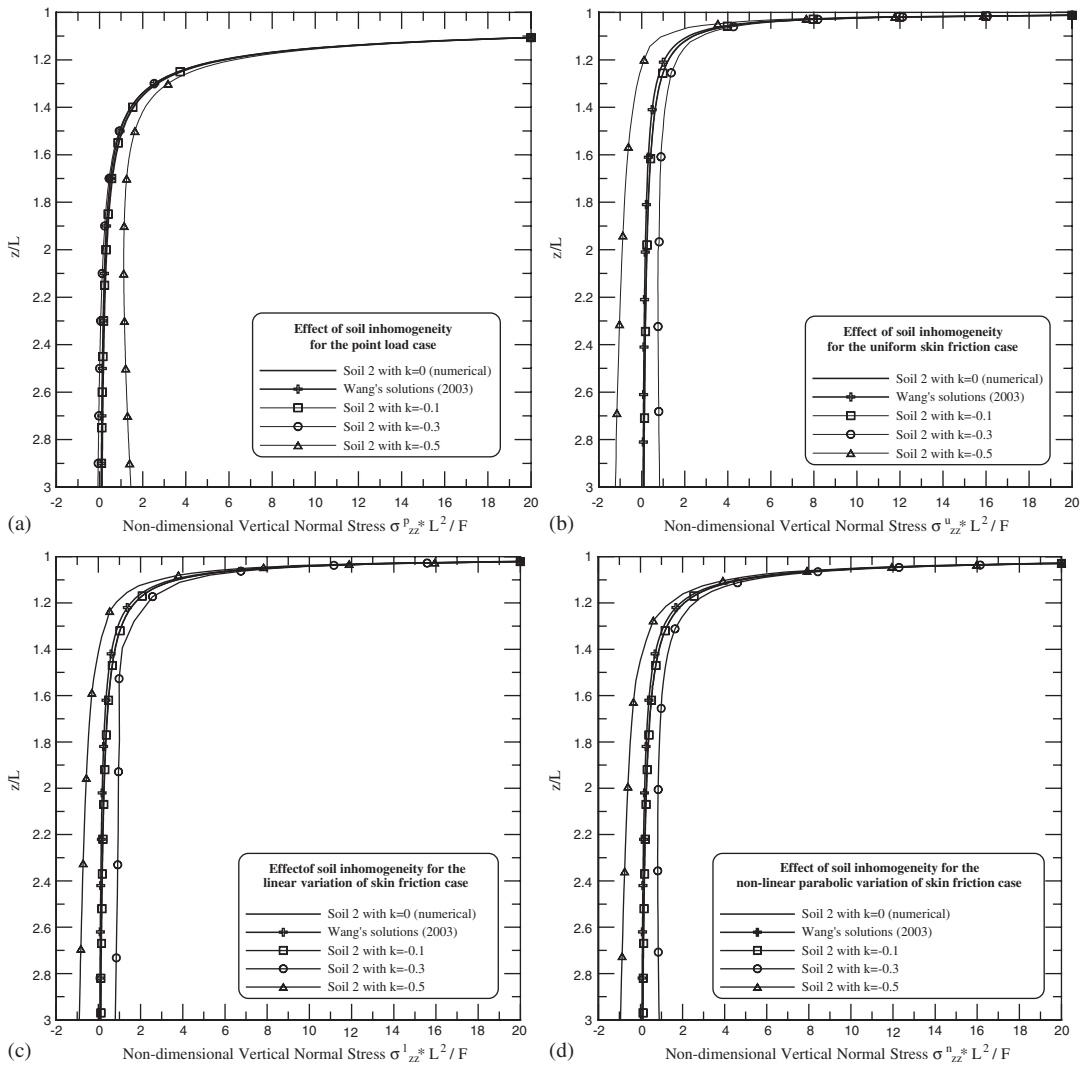

Figure 7. Effect of soil inhomogeneity. Variation of non-dimensional vertical normal stress with non-dimensional depth below the loading line in inhomogeneous Soil 2: Point load in (a); uniform skin friction in (b); linear variation of skin friction in (c); and non-linear parabolic variation of skin friction in (d).

$$\tau_{rz}^{u*} = \frac{-F}{4\pi C_{33} L}\left\{ -B_1 \frac{1}{u_1 \xi}[e^{-u_1\xi z} - e^{-u_1\xi(z-L)}] + B_2 \frac{1}{(k-u_2\xi)}[e^{(k-u_2\xi)z} - e^{(k-u_2\xi)(z-L)}] \right.$$
$$+ B_1 \frac{\Delta_1}{\Delta}\frac{1}{u_1\xi}[e^{-u_1\xi z} - e^{-u_1\xi(z+L)}] + B_3 \frac{\Delta_2}{\Delta}\frac{1}{u_2\xi}(1 - e^{-u_2\xi L})e^{(k-u_1\xi)z}$$
$$\left. + B_4 \frac{\Delta_3}{\Delta}\frac{1}{u_1\xi}(1 - e^{-u_1\xi L})e^{(k-u_2\xi)z} - B_2\frac{\Delta_4}{\Delta}\frac{1}{(k-u_2\xi)}[e^{(k-u_2\xi)z} - e^{(k-u_2\xi)(z+L)}] \right\} \quad (13)$$

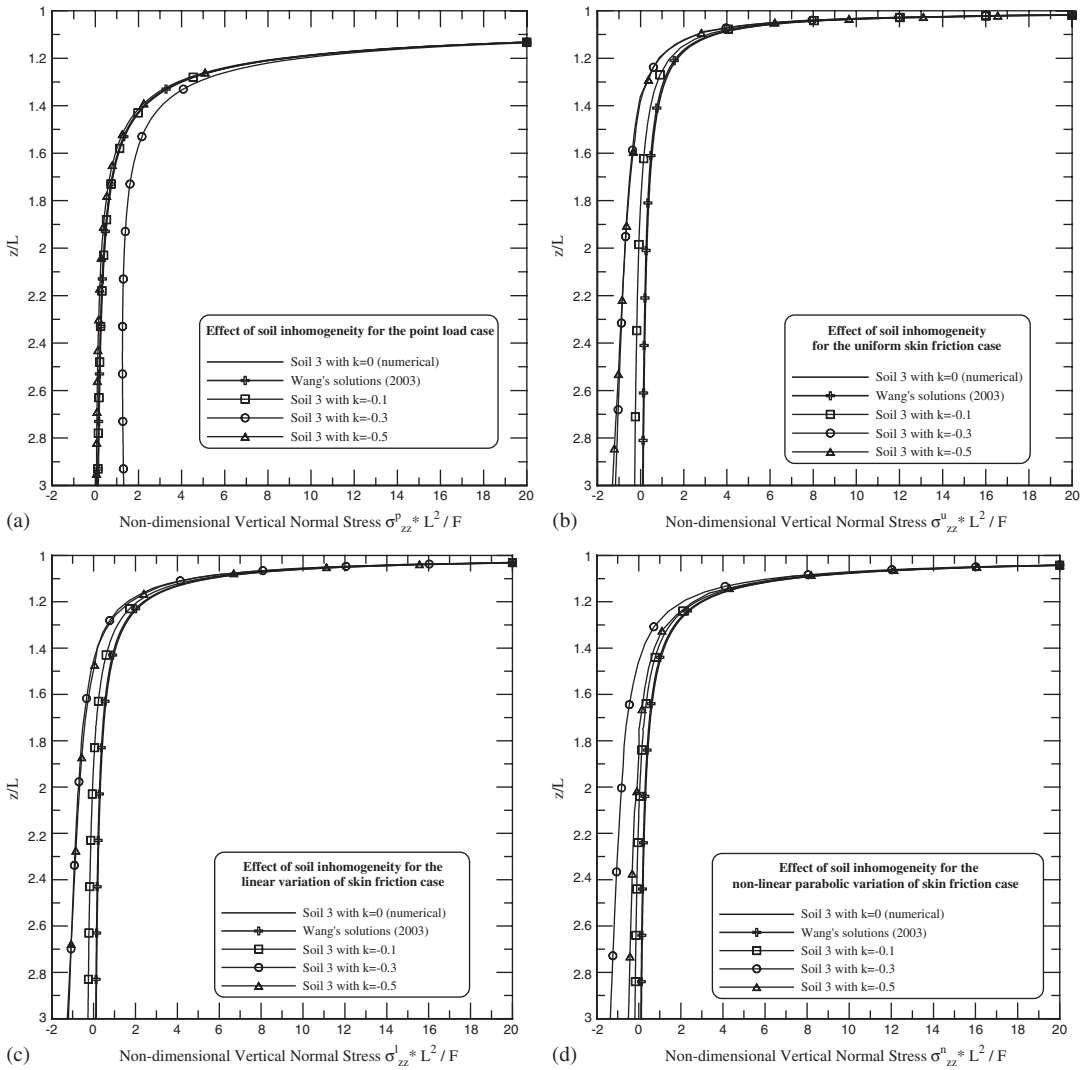

Figure 8. Effect of soil inhomogeneity. Variation of non-dimensional vertical normal stress with non-dimensional depth below the loading line in inhomogeneous Soil 3: Point load in (a); uniform skin friction in (b); linear variation of skin friction in (c); and non-linear parabolic variation of skin friction in (d).

where σ^{u*}_{zz} and τ^{u*}_{rz} denote the vertical normal and shear stresses in the Hankel-transformed domain. The physical domain stresses are found by taking the inverse Hankel transforms, i.e.

$$\begin{Bmatrix} \sigma^{u}_{zz} \\ \tau^{u}_{rz} \end{Bmatrix} = \int_0^{\infty} \xi \begin{Bmatrix} \sigma^{u*}_{zz} J_0(\xi r) \\ \tau^{u*}_{rz} J_1(\xi r) \end{Bmatrix} \mathrm{d}\xi \tag{14}$$

where σ^{u}_{zz} and τ^{u}_{rz} are the vertical normal and shear stresses in the physical domain due to the uniform skin friction. We remark that these expressions reduce to Geddes's/Wang's solutions [5, 7] if the half-space is homogeneous and isotropic/cross-anisotropic, respectively.

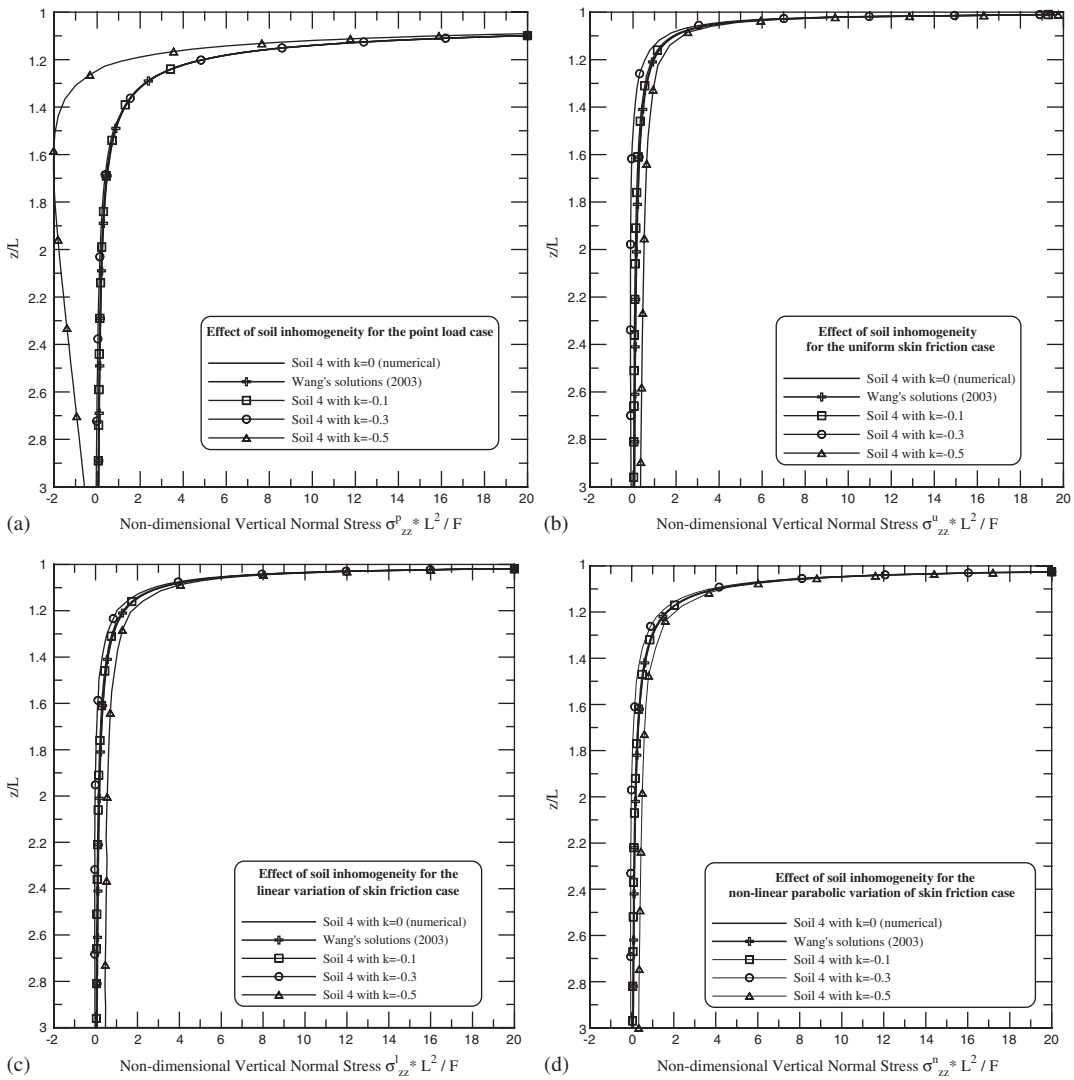

Figure 9. Effect of soil inhomogeneity. Variation of non-dimensional vertical normal stress with non-dimensional depth below the loading line in inhomogeneous Soil 4: Point load in (a); uniform skin friction in (b); linear variation of skin friction in (c); and non-linear parabolic variation of skin friction in (d).

CASE C: STRESSES DUE TO A LINEAR VARIATION OF SKIN FRICTION

The linearly varying skin friction assumed for a total load of Q (force per unit length) is shown in Figure 4. The load applied over a depth $d\eta$ is given by:

$$dQ = 2F\left(\frac{\eta}{L^2}\right)d\eta \tag{15}$$

Following the same approach as for Case B, i.e. substituting Equation (15) into Equations (1)–(2), and integrating η from 0 to L gives the following expression:

$$\begin{aligned}\sigma_{zz}^{\mathrm{I}^*} = &\frac{F}{2\pi C_{33}C_{44}L^2}\left\{A_1\frac{1}{u_1^2\xi^2}[\mathrm{e}^{-u_1\xi z}-(1-u_1\xi L)\mathrm{e}^{-u_1\xi(z-L)}]\right.\\ &+A_2\frac{1}{(k-u_2\xi)^2}\{\mathrm{e}^{(k-u_2\xi)z}-[1+(k-u_2\xi)L]\mathrm{e}^{(k-u_2\xi)(z-L)}\}\\ &-A_1\frac{\Delta_1}{\Delta}\frac{1}{u_1^2\xi^2}[\mathrm{e}^{-u_1\xi z}-(1+u_1\xi L)\mathrm{e}^{-u_1\xi(z+L)}]\\ &-A_3\frac{\Delta_2}{\Delta}\frac{1}{u_2^2\xi^2}[1-(1+u_2\xi L)\mathrm{e}^{-u_2\xi L}]\mathrm{e}^{(k-u_1\xi)z}\\ &-A_4\frac{\Delta_3}{\Delta}\frac{1}{u_1^2\xi^2}[1-(1+u_1\xi L)\mathrm{e}^{-u_1\xi L}]\mathrm{e}^{(k-u_2\xi)z}\\ &\left.-A_2\frac{\Delta_4}{\Delta}\frac{1}{(k-u_2\xi)^2}\{\mathrm{e}^{(k-u_2\xi)z}-[1-(k-u_2\xi)L]\mathrm{e}^{(k-u_2\xi)(z+L)}\}\right\}\end{aligned} \tag{16}$$

$$\begin{aligned}\tau_{rz}^{\mathrm{I}^*} = &\frac{-F}{2\pi C_{33}L^2}\left\{B_1\frac{1}{u_1^2\xi^2}[\mathrm{e}^{-u_1\xi z}-(1-u_1\xi L)\mathrm{e}^{-u_1\xi(z-L)}]\right.\\ &+B_2\frac{1}{(k-u_2\xi)^2}\{\mathrm{e}^{(k-u_2\xi)z}-[1+(k-u_2\xi)L]\mathrm{e}^{(k-u_2\xi)(z-L)}\}\\ &+\mathrm{B}_1\frac{\Delta_1}{\Delta}\frac{1}{u_1^2\xi^2}[\mathrm{e}^{-u_1\xi z}-(1+u_1\xi L)\mathrm{e}^{-u_1\xi(z+L)}]\\ &+B_3\frac{\Delta_2}{\Delta}\frac{1}{u_2^2\xi^2}[1-(1+u_2\xi L)\mathrm{e}^{-u_2\xi L}]\mathrm{e}^{(k-u_1\xi)z}\\ &+\mathrm{B}_4\frac{\Delta_3}{\Delta}\frac{1}{u_1^2\xi^2}[1-(1+u_1\xi L)\mathrm{e}^{-u_1\xi L}]\mathrm{e}^{(k-u_2\xi)z}\\ &\left.+\mathrm{B}_2\frac{\Delta_4}{\Delta}\frac{1}{(k-u_2\xi)^2}\{\mathrm{e}^{(k-u_2\xi)z}-[1-(k-u_2\xi)L]\mathrm{e}^{(k-u_2\xi)(z+L)}\}\right\}\end{aligned} \tag{17}$$

where $\sigma_{zz}^{\mathrm{I}^*}$ and $\tau_{rz}^{\mathrm{I}^*}$ are the vertical normal and shear stresses in the Hankel-transformed domain. Similarly, the stresses in the physical domain $(\sigma_{zz}^{\mathrm{I}}, \tau_{rz}^{\mathrm{I}})$ are obtained via numerical integral of

$$\begin{Bmatrix}\sigma_{zz}^{\mathrm{I}}\\ \tau_{rz}^{\mathrm{I}}\end{Bmatrix} = \int_0^\infty \xi \begin{Bmatrix}\sigma_{zz}^{\mathrm{I}^*}J_0(\xi r)\\ \tau_{rz}^{\mathrm{I}^*}J_1(\xi r)\end{Bmatrix}\mathrm{d}\xi \tag{18}$$

Again, if the half-space is homogeneous and isotropic/cross-anisotropic, Equation (18) is reduced to Geddes's/Wang's solutions [5, 7], respectively.

CASE D: STRESSES DUE TO A NON-LINEAR PARABOLIC VARIATION OF SKIN FRICTION

A total load of Q (force per unit length), applied along the vertical axis z in increments varying non-linearly parabolic with depth, from zero at the surface to a maximum at depth L is investigated (Figure 5). The incremental load $\mathrm{d}Q$ over a depth $\mathrm{d}\eta$ can be expressed as:

$$\mathrm{d}Q = 3F\left(\frac{\eta^2}{L^3}\right)\mathrm{d}\eta \tag{19}$$

Substituting Equation (19) into Equations (1)–(2) and integrating the result for η from 0 to L gives the following expression:

$$\begin{aligned}\sigma_{zz}^{n*} = \frac{3F}{4\pi C_{33}C_{44}L^3}\Bigg\{ & -A_1\frac{1}{u_1^3\xi^3}[2\mathrm{e}^{-u_1\xi z} - (2-2u_1\xi L + u_1^2\xi^2L^2)\mathrm{e}^{-u_1\xi(z-L)}] \\ & + A_2\frac{1}{(k-u_2\xi)^3}\{2\mathrm{e}^{(k-u_2\xi)z} - [2+2(k-u_2\xi)L + (k-u_2\xi)^2L^2]\mathrm{e}^{(k-u_2\xi)(z-L)}\} \\ & - A_1\frac{\Delta_1}{\Delta}\frac{1}{u_1^3\xi^3}[2\mathrm{e}^{-u_1\xi z} - (2+2u_1\xi L + u_1^2\xi^2L^2)\mathrm{e}^{-u_1\xi(z+L)}] \\ & - A_3\frac{\Delta_2}{\Delta}\frac{1}{u_2^3\xi^3}[2-(2+2u_2\xi L + u_2^2\xi^2L^2)\mathrm{e}^{-u_2\xi L}]\mathrm{e}^{(k-u_1\xi)z} \\ & - A_4\frac{\Delta_3}{\Delta}\frac{1}{u_1^3\xi^3}[2-(2+2u_1\xi L + u_1^2\xi^2L^2)\mathrm{e}^{-u_1\xi L}]\mathrm{e}^{(k-u_2\xi)z} \\ & + A_2\frac{\Delta_4}{\Delta}\frac{1}{(k-u_2\xi)^3}\{2\mathrm{e}^{(k-u_2\xi)z} - [2-2(k-u_2\xi)L + (k-u_2\xi)^2L^2]\mathrm{e}^{(k-u_2\xi)(z+L)}\}\Bigg\}\end{aligned} \tag{20}$$

$$\begin{aligned}\tau_{rz}^{n*} = \frac{-3F}{4\pi C_{33}L^3}\Bigg\{ & -B_1\frac{1}{u_1^3\xi^3}[2\mathrm{e}^{-u_1\xi z} - (2-2u_1\xi L + u_1^2\xi^2L^2)\mathrm{e}^{-u_1\xi(z-L)}] \\ & + B_2\frac{1}{(k-u_2\xi)^3}\{2\mathrm{e}^{(k-u_2\xi)z} - [2+2(k-u_2\xi)L + (k-u_2\xi)^2L^2]\mathrm{e}^{(k-u_2\xi)(z-L)}\} \\ & + B_1\frac{\Delta_1}{\Delta}\frac{1}{u_1^3\xi^3}[2\mathrm{e}^{-u_1\xi z} - (2+2u_1\xi L + u_1^2\xi^2L^2)\mathrm{e}^{-u_1\xi(z+L)}] \\ & + B_3\frac{\Delta_2}{\Delta}\frac{1}{u_2^3\xi^3}[2-(2+2u_2\xi L + u_2^2\xi^2L^2)\mathrm{e}^{-u_2\xi L}]\mathrm{e}^{(k-u_1\xi)z} \\ & + B_4\frac{\Delta_3}{\Delta}\frac{1}{u_1^3\xi^3}[2-(2+2u_1\xi L + u_1^2\xi^2L^2)\mathrm{e}^{-u_1\xi L}]\mathrm{e}^{(k-u_2\xi)z} \\ & - B_2\frac{\Delta_4}{\Delta}\frac{1}{(k-u_2\xi)^3}\{2\mathrm{e}^{(k-u_2\xi)z} - [2-2(k-u_2\xi)L + (k-u_2\xi)^2L^2]\mathrm{e}^{(k-u_2\xi)(z+L)}\}\Bigg\}\end{aligned} \tag{21}$$

where σ_{zz}^{n*} and τ_{rz}^{n*} represent the stress components in the Hankel-transformed domain. The stresses in the physical domain ($\sigma_{zz}^{n}, \tau_{rz}^{n}$) are expressed as follows:

$$\begin{Bmatrix} \sigma_{zz}^{n} \\ \tau_{rz}^{n} \end{Bmatrix} = \int_0^\infty \xi \begin{Bmatrix} \sigma_{zz}^{n*} J_0(\xi r) \\ \tau_{rz}^{n*} J_1(\xi r) \end{Bmatrix} \mathrm{d}\xi \tag{22}$$

Since no analytical solution for this loading case is available for a homogeneous and isotropic half-space, the numerical results for an isotropic medium are examined by utilizing the closed-form solutions of Wang [7] via a limiting process. It is found that the results obtained using the presented solution are in full agreement with Wang's solutions [7] if the half-space is homogeneous and isotropic/cross-anisotropic.

ILLUSTRATIVE EXAMPLES

A parametric study is conducted to verify the solutions and to investigate the effect of material inhomogeneity, the type and degree of material anisotropy, and the loading types on the vertical normal stress. For typical ranges of cross-anisotropic parameters, Gazetas [14] summarized several experimental data regarding deformational cross-anisotropy of clays and sands. He concluded that the ratio E/E' ranged from 0.6 to 4 for clays and was as low as 0.2 for sands. For the heavily over-consolidated London clay, however, the ratio for E/E' is in the range 1.35–2.37 and for G'/E' is in 0.23–0.44 [15–18]. Besides, the hypothetical ratio v/v' varying between 0.75 and 1.5 is the possible range of the Poisson's ratios [7]. Hence, the degree of anisotropy of London clay, including the ratios $E/E', G'/E'$, and v/v', is accounted for investigating its effect on the stress. The elastic properties for several types of isotropic and cross-anisotropic soils as foregoing mentioned are listed in Table II. The values adopted in Table II for E and v are 50 MPa and 0.3, respectively.

Based on Equations (1), (2), (5) (for a point load), Equations (12)–(14) (for a uniform skin friction), Equations (16)–(18) (for linear variation of skin friction), and Equations (20)–(22) (for non-linear parabolic variation of skin friction), a FORTRAN program was written to calculate the stresses. In the program, the vertical normal and shear stresses at any point in the half-space can be computed. However, the vertical normal stress is of greater significance in practical problems; hence, numerical results are shown only for this component at the depth z below the pile tip ($z/L > 1$). According to the results reported in Figures 6–14, the effect of the soil inhomogeneity, the type and degree of soil anisotropy, and the loading types on the vertical normal stress is investigated below.

Firstly, the non-dimensional vertical normal stress ($\sigma_{zz}^{p*} L^2/F$, $\sigma_{zz}^{u*} L^2/F$, $\sigma_{zz}^{l*} L^2/F$, $\sigma_{zz}^{n*} L^2/F$) for Soils 1–4 (Table II) below the line of load ($r = 0$) resulted from a point load, a uniform skin

Table II. Elastic coefficients for different soils ($E = 50$ MPa, $v = 0.3$).

Soil type	E/E'	G'/E'	v/v'
Soil 1. Isotropy	1.0	0.385	1.0
Soil 2. Cross-anisotropy	2.37	0.385	1.0
Soil 3. Cross-anisotropy	1.0	0.23	1.0
Soil 4. Cross-anisotropy	1.0	0.385	1.5

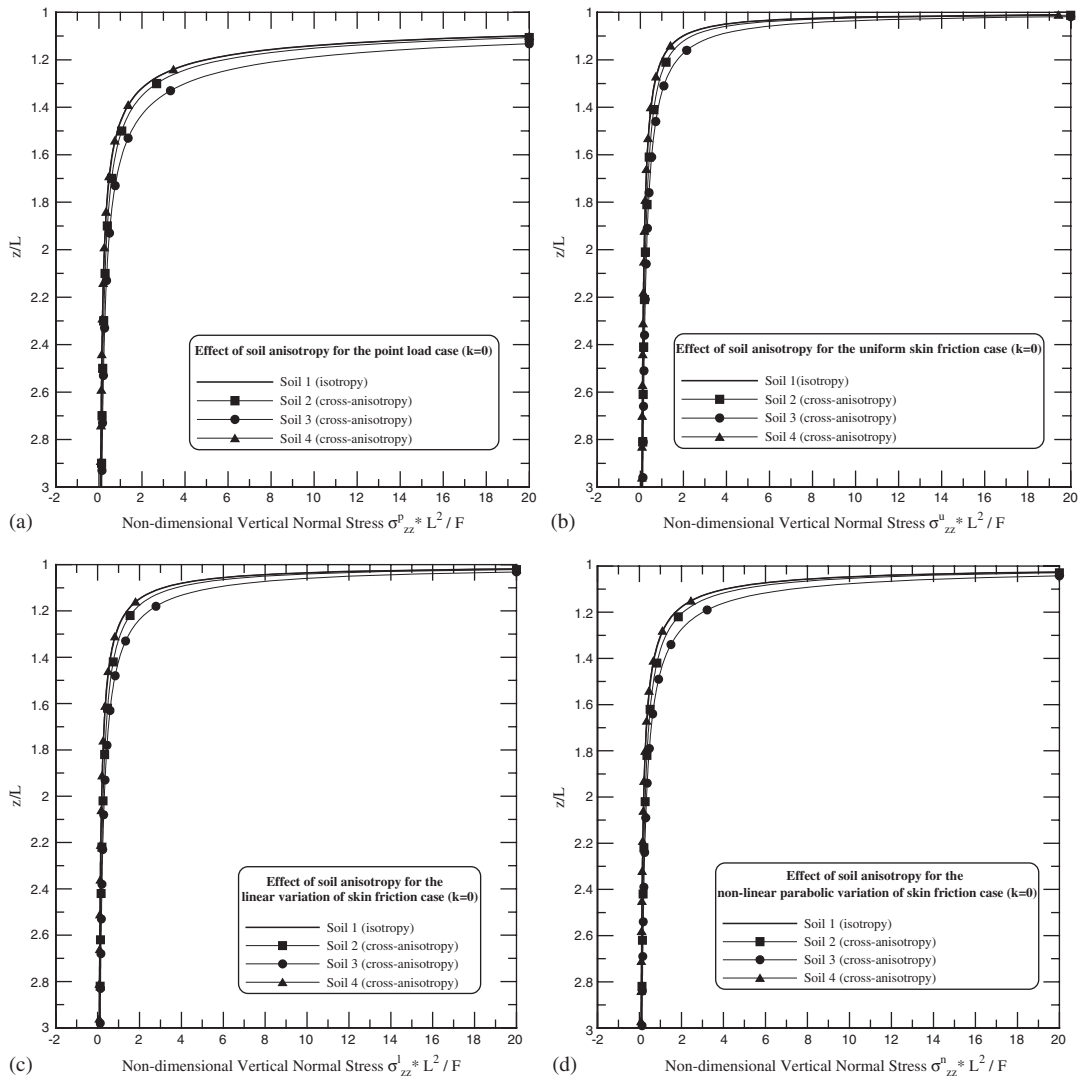

Figure 10. Effect of soil anisotropy. Variation of non-dimensional vertical normal stress with non-dimensional depth below the loading line in Soils 1–4 for $k = 0$: Point load in (a); uniform skin friction in (b); linear variation of skin friction in (c); and non-linear parabolic variation of skin friction in (d).

friction, a linear variation of skin friction, and a non-linear parabolic variation of skin friction vs the non-dimensional ratio z/L is given in Figures 6(a)–6(d), Figures 7(a)–7(d), Figures 8(a)–8(d), and Figures 9(a)–9(d), respectively. In order to check the accuracy of the proposed solutions, comparisons with the homogeneous and isotropic solutions of Mindlin [3] and Geddes [5], and homogeneous and cross-anisotropic solutions of Wang [7], are also carried out by a limiting procedure. The results based on the presented numerical techniques are in good agreement with previous ones [3, 5, 7]. The inhomogeneity parameter k is chosen to

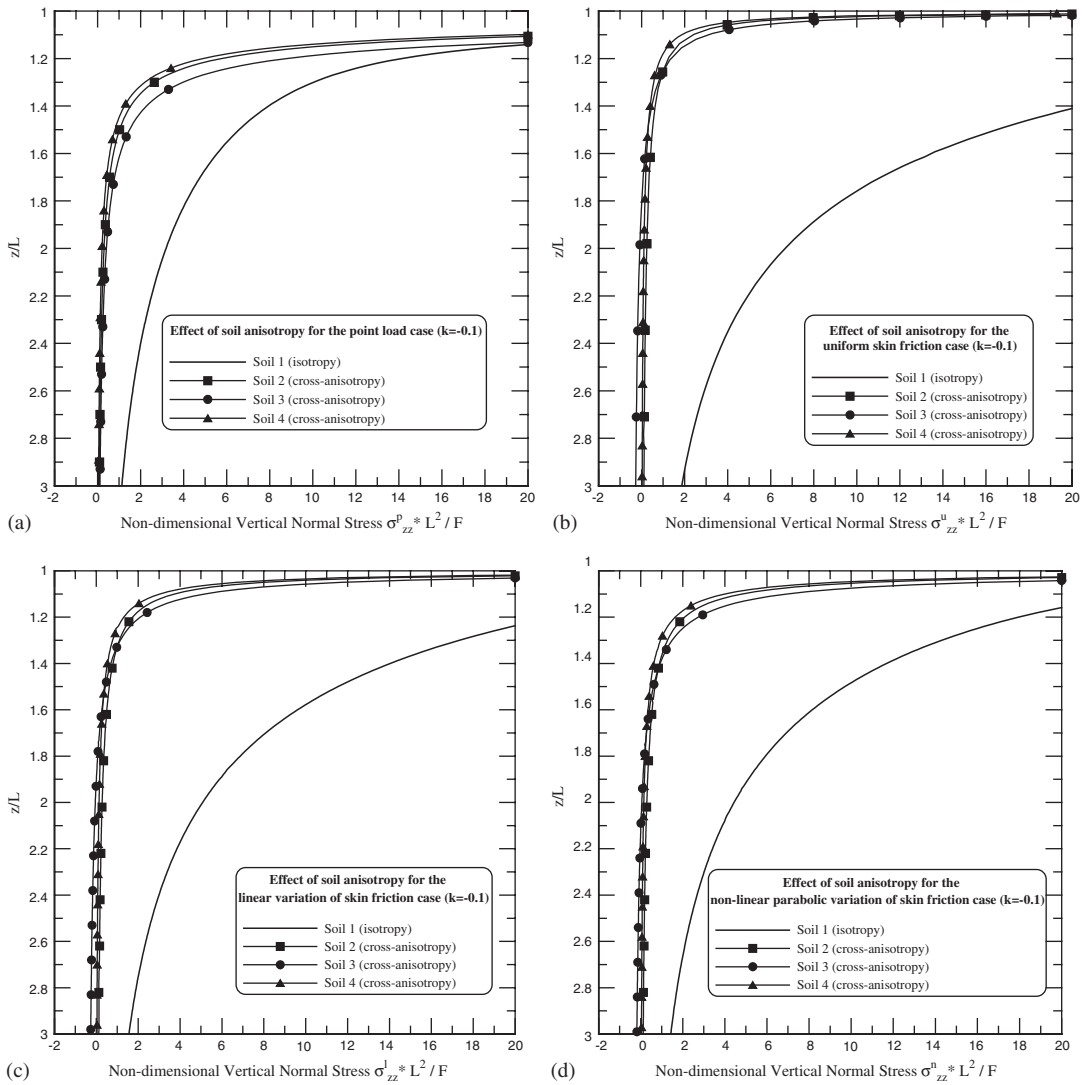

Figure 11. Effect of soil anisotropy. Variation of non-dimensional vertical normal stress with non-dimensional depth below the loading line in Soils 1–4 for $k = -0.1$: Point load in (a); uniform skin friction in (b); linear variation of skin friction in (c); and non-linear parabolic variation of skin friction in (d).

vary from 0 (homogeneous) to $-0.5 (k < 0$, denotes a soft surface, whereas E, E', G' increase with the increase of depth). Figures 6(a)–6(d) indicate that for the given pile length (L) and loading type (point load in Figure 6(a), uniform skin friction in Figure 6(b), linear variation of skin friction in Figure 6(c), and non-linear parabolic variation of skin friction in Figure 6(d)), the stress variation with the depth (z) has similar trends for Soil 1 (isotropy, $E/E' = 1.0,\ G'/E' = 0.385, v/v' = 1.0$). In particular, the magnitude of the induced vertical normal stress in Soil 1 by each loading case decreases with the increasing z/L (from 1 to 3), and

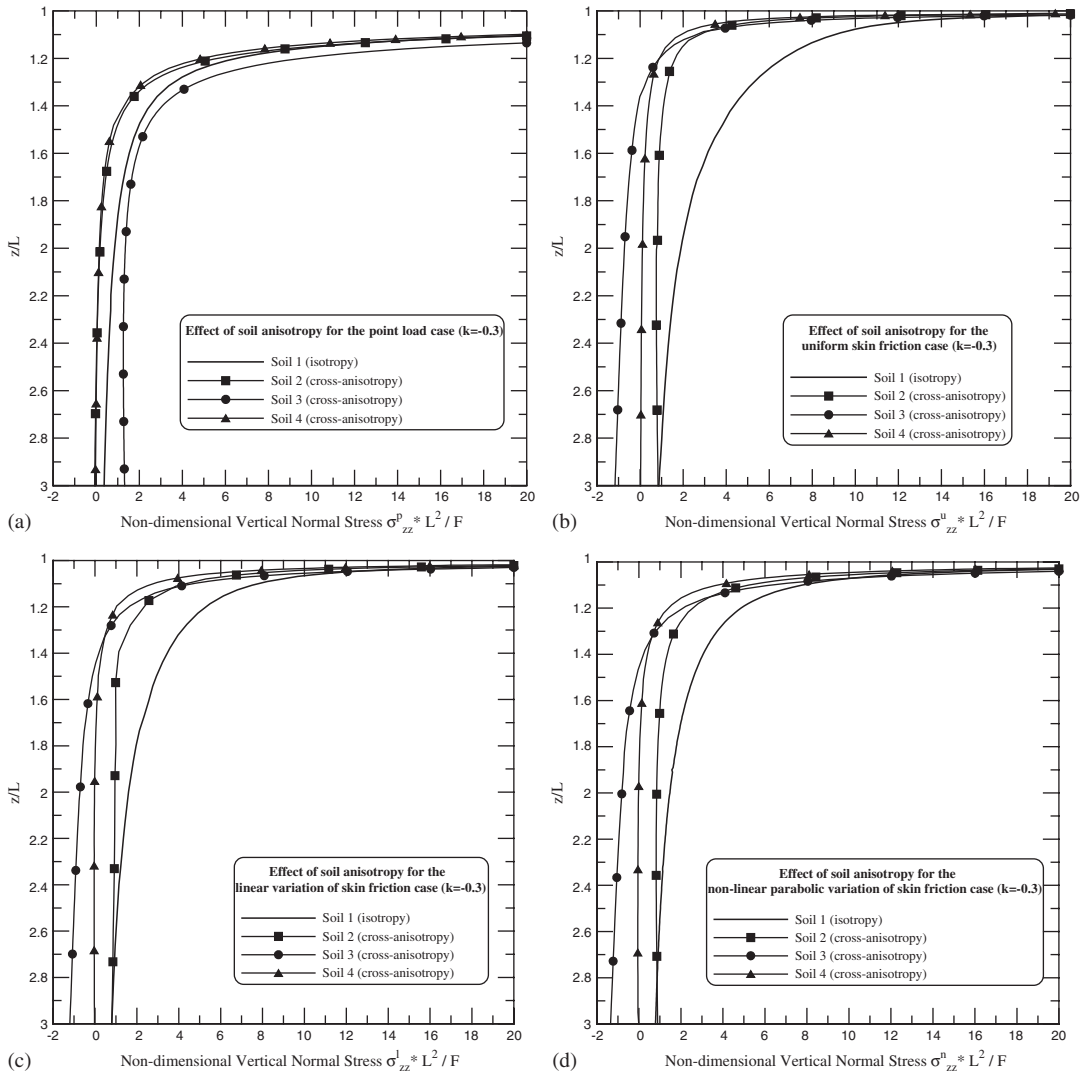

Figure 12. Effect of soil anisotropy. Variation of non-dimensional vertical normal stress with non-dimensional depth below the loading line in Soils 1–4 for $k = -0.3$: Point load in (a); uniform skin friction in (b); linear variation of skin friction in (c); and non-linear parabolic variation of skin friction in (d).

it obeys the order (from large to small): $k = -0.1 > k = -0.3 > k = -0.5 > k = 0$ ($k < 0, E, E'$, G' increase with the increasing depth). Figures 7–9 show the induced stress by the four different loading types for Soil 2 (cross-anisotropy, $E/E' = 2.37, G'/E' = 0.385, v/v' = 1.0$), Soil 3 (cross-anisotropy, $E/E' = 1.0$, $G'/E' = 0.23, v/v' = 1.0$), and Soil 4 (cross-anisotropy, $E/E' = 1.0$, $G'/E' = 0.385, v/v' = 1.5$), respectively. It is interesting that for Soil 2 with $k = -0.5$, while a non-zero compressive stress may still exist at a relatively large depth (i.e., $z/L > 3$) when the soil is under the point load (Figure 7(a)), the induced vertical normal stress might be transferred to

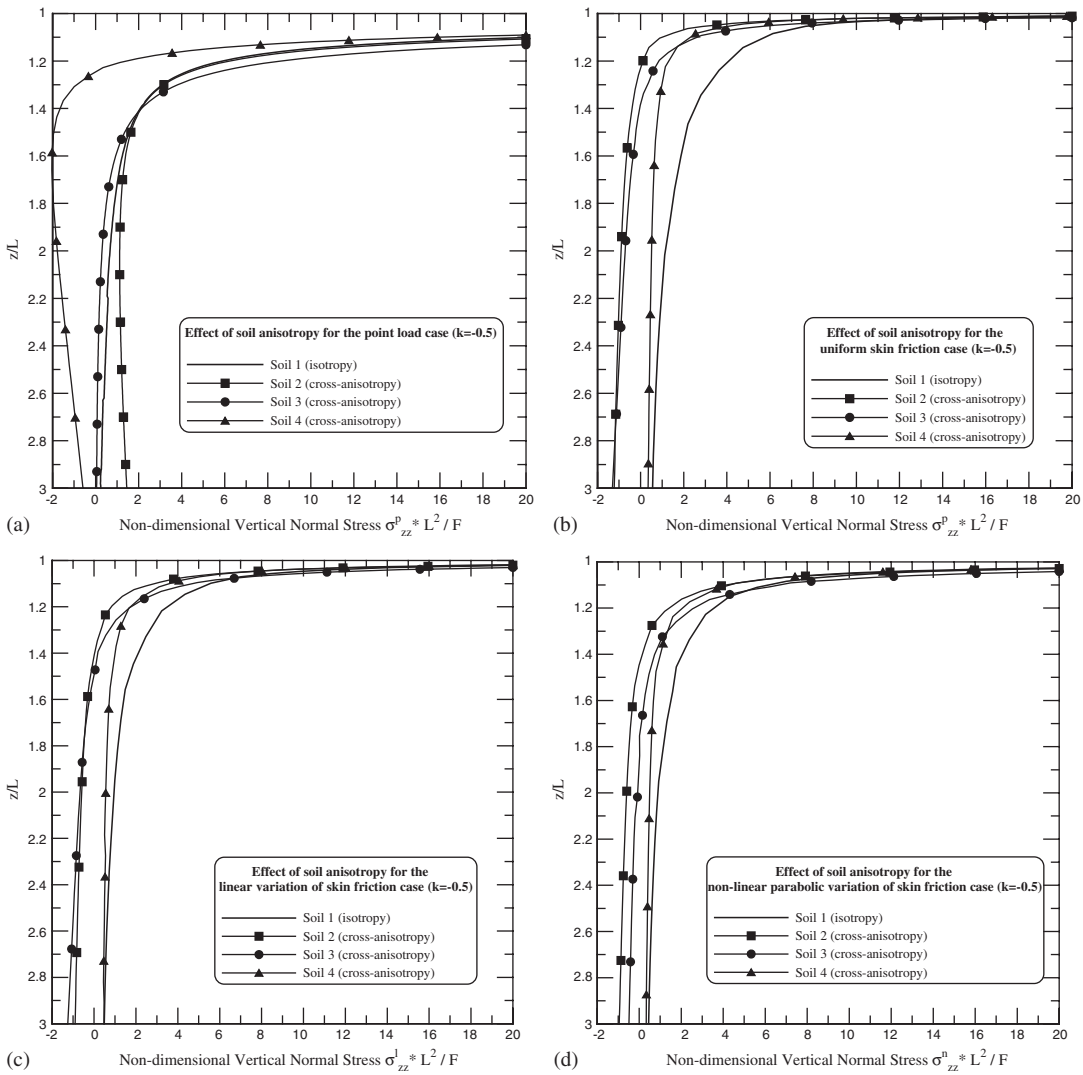

Figure 13. Effect of soil anisotropy. Variation of non-dimensional vertical normal stress with non-dimensional depth below the loading line in Soils 1–4 for $k = -0.5$: Point load in (a); uniform skin friction in (b); linear variation of skin friction in (c); and non-linear parabolic variation of skin friction in (d).

tensile for the skin friction cases at $z/L > 1.4$ (Figures 7(b)–(d)). For Soil 3 shown in Figures 8(b)–8(d), the stress distribution is similar to that for Soil 2, with the inhomogeneity parameter k at -0.3, instead of -0.5 for Soil 2. Figures 9(b)–9(d) plot the stress distribution for Soil 4. It is observed that different skin friction cases predict nearly identical and close-to-zero vertical normal stress, except for the point load case when $k = -0.5$.

Secondly, the non-dimensional vertical normal stress vs z/L for the inhomogeneity parameter $k = 0, -0.1, -0.3$, and -0.5, also resulted from the presented loading types, is given in

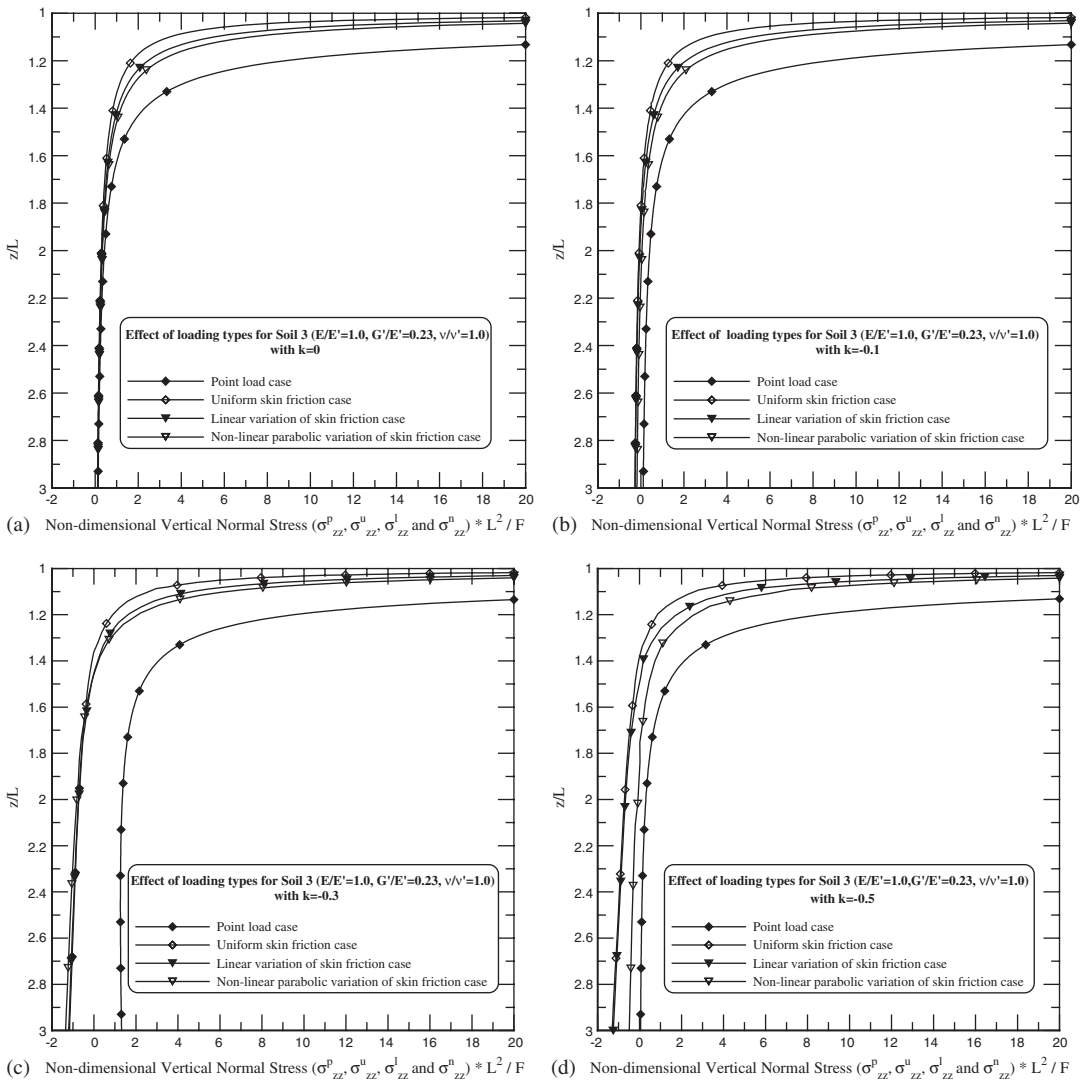

Figure 14. Effect of loading types. Variation of non-dimensional vertical normal stress with non-dimensional depth below the loading line in Soil 3: $k = 0$ in (a); $k = -0.1$ in (b); $k = -0.3$ in (c); and $k = -0.5$ in (d).

Figures 10(a)–10(d), 11(a)–11(d), 12(a)–12(d), and 13(a)–13(d), respectively. Figures 10(a)–10(d) show that for $k = 0$ (homogeneous and isotropic soil (Soil 1), and homogeneous and cross-anisotropic soils (Soils 2–4)), the magnitude of induced vertical normal stress by each loading case decreases with increasing z/L (from 1 to 3), and follows the order: Soil 3 > Soil 2 > Soil 1 = Soil 4. In other words, the ratio v/v' (Soil 4, $E/E' = 1.0$, $G'/E' = 0.385$, $v/v' = 1.5$) has nearly no influence on the stress. We also found that the variation of the stress in different soils is very small when $z/L > 2$. From Figures 11(a)–11(d), we observed that for $k = -0.1$, the stress

in the isotropic soil (i.e. Soil 1) for all the loading cases is considerably larger than that in the cross-anisotropic soils (i.e. Soils 2–4). For $k = -0.3$ and -0.5, however, the feature of the stress distribution becomes complicated (Figures 12 and 13). The stress induced by the skin friction loads for $k = -0.3$ becomes tensile for Soil 3 when $z/L > 1.4$ (Figures 12(b)–12(d)), whereas for $k = -0.5$ it becomes tensile in both Soils 2 and 3 when $z/L > 1.5$ (Figures 13(b)–13(d)). We also noticed that the stress induced by the point load for $k = -0.5$ can be tensile in Soil 4 (Figure 13(a)).

Finally, Figure 14 illustrates the effect of different loading types on the induced vertical normal stress in Soil 3 (cross-anisotropy, $E/E' = 1.0$, $G'/E' = 0.23, v/v' = 1.0$). From Figure 14(a), we observed that, when $k = 0$, the stress quickly approaches to zero for all the loading types; however, a non-zero vertical normal stress can exist even when $z/L > 3$ (Figures 14(b)–14(d)). Perhaps the most interesting feature is that for $k = -0.1, -0.3$ and -0.5, a tensile stress can be induced when the soil is under the skin friction loads (Figures 14(b)–14(d)). It is clear that the magnitude of vertical normal stress strongly depends on the soil inhomogeneity, particularly when $k = -0.3$ or -0.5.

CONCLUSIONS AND DISCUSSIONS

In this article, solutions are presented for the vertical normal and shear stresses induced by various loadings associated with a pile in a continuously inhomogeneous and cross-anisotropic half-space. The planes of cross-anisotropy are parallel to the surface of the half-space and the Young's and shear moduli in the half-space are assumed to vary exponentially with depth. The loading types include an embedded point load for an end-bearing pile, and the uniform skin friction, linear variation of skin friction, and non-linear parabolic variation of skin friction for a friction pile, respectively. These solutions are expressed in terms of the Hankel transform using the recently developed point load solutions [10]. Numerical techniques are proposed to carry out the inverse Hankel transform. It is shown that the stresses predicted based on the presented formulation for the special cases are in good agreement with previous published results. These include the homogeneous isotropic solutions of Geddes [5] for a point load (the same as the Mindlin's solution [3]), a uniform skin friction, and linear variation of skin friction when the medium is isotropic. They also include the homogeneous cross-anisotropic solutions of Wang [7] for the four different loads when the medium is cross-anisotropic. Furthermore, parametric studies are carried out for London clay and some interesting results are summarized as follows:

1. For the isotropic Soil 1 (Figure 6), the magnitudes of the induced vertical normal stresses by each loading decrease with increasing depth z/L (from 1 to 3), and the stresses are all under compression.
2. For the cross-anisotropic Soil 2 (Figure 7), tensile stress can be induced in the inhomogeneous soil for the soft surface case ($k = -0.5$) at depth $z/L > 1.4$ for the three skin friction loads. For the point load case, the corresponding stress is compressive. Furthermore, the $k = -0.3$ case gives a non-zero compressive stress for the three skin friction loads.
3. For the cross-anisotropic Soil 3 (Figure 8), the stress distribution is similar to that for Soil 2 (Figure 7), but here the same tend holds for $k = -0.3$, instead of $k = -0.5$.
4. For the cross-anisotropic Soil 4 (Figure 9), except for the point load case where the stress corresponding to $k = -0.5$ is tensile in most part of the depth z/L from 1 to 3, the stresses for other cases are very close to zero.

5. For the homogeneous case, $k = 0$ (Figure 10), the stresses for all the cases are very close to zero for $z/L > 2$.
6. For the given inhomogeneity parameter $k = -0.1$ (Figure 11), except for the isotropic soil where a large compressive stress exists even for $z/L > 2$, the stresses for other cases are very close to zero (for $z/L > 2$).
7. For the given inhomogeneity parameter $k = -0.3$ (Figure 12), except for the point load case where a non-zero compressive stress exists, the stresses in Soil 3 are tensile for $z/L >$ 1.4. It is also noted that the stresses due to the skin friction loads in Soils 1 and 2 are compressive, and in Soil 4, the stress is negligible.
8. For the given inhomogeneity parameter $k = -0.5$ (Figure 13), tensile stress develops in Soils 2 and 3 when under skin friction loads.
9. For the given inhomogeneous cross-anisotropic Soil 3 (Figure 14), tensile stress can be developed if the soil is under skin friction loads, especially when $k = -0.3$ or -0.5.

While this article has been concerned with the stresses of single piles in an inhomogeneous and cross-anisotropic half-space, the method of analysis utilized herein can be conveniently applied to the analysis of settlements or both of pile groups by using the principle of superposition. Also, the presented point load solutions can be extended to simulate the pile-soil-pile as well as pile group-pile cap interaction problems. These solutions could more realistically imitate the actual stratum of loading situations in many areas of engineering practice, and provide a mathematical model to the problems in soil/rock mechanics and piling engineering where the media are of inhomogeneity and cross-anisotropy.

APPENDIX A: NOMENCLATURE

C_{ij} $(i,j = 1–6)$	elastic moduli of the medium
$d\eta$	infinitesimal element along the z-axis
E	Young's modulus in the horizontal direction
E'	Young's modulus in the vertical direction
F	force for an end-bearing or a friction pile
G'	shear modulus in the vertical plane
$J_n(\,)$	Bessel function of the first kind of order n
k	the inhomogeneity parameter, as in e^{-kz}
L	the pile length
Q	total load (force per unit length)
u_1, u_2	roots of the characteristic equation

Greek letters

η	the buried depth, as seen in Figure 1
v	Poisson's ratio characterizing the effect of horizontal stress on the complementary horizontal strain
v'	Poisson's ratio characterizing the effect of vertical stress on the horizontal strain
$\sigma_{zz}^{1}, \tau_{rz}^{1}$	stresses in the physical domain, due to the linear variation of skin friction
$\sigma_{zz}^{1*}, \tau_{rz}^{1*}$	stresses in the Hankel-transformed domain, due to the linear variation of skin friction

$\sigma_{zz}^{n}, \tau_{rz}^{n}$	stresses in the physical domain, due to the non-linear parabolic variation of skin friction
$\sigma_{zz}^{n*}, \tau_{rz}^{n*}$	stresses in the Hankel-transformed domain, due to the non-linear parabolic variation of skin friction
$\sigma_{zz}^{p}, \tau_{rz}^{p}$	stresses in the physical domain, due to a point load
$\sigma_{zz}^{p*}, \tau_{rz}^{p*}$	stresses in the Hankel-transformed domain, due to a point load
$\sigma_{zz}^{u}, \tau_{rz}^{u}$	stresses in the physical domain, due to the uniform skin friction
$\sigma_{zz}^{u*}, \tau_{rz}^{u*}$	stresses in the Hankel-transformed domain, due to the uniform skin friction

ACKNOWLEDGEMENTS

The authors wish to thank C. S. Tzeng, and Professor J. J. Liao (Department of Civil Engineering, National Chiao-Tung University, R.O.C.) for their great contributions to the point load solutions of an inhomogeneous cross-anisotropic half-space utilized in this paper [10].

REFERENCES

1. Suresh S. Graded materials for resistance to contact deformation and damage. *Science* 2001; **292**:2447–2451.
2. ITASCA Consulting Group Inc. FLAC-Fast lagrangian analysis of continua. Minneapolis, MN, U.S.A., 1999.
3. Mindlin RD. Force at a point in the interior of a semi-infinite solid. *Physics* 2001; **7**(5):195–202.
4. Grillo O. Influence scale and influence chart for the computation of stresses due respectively to surface point load and pile load. *Proceedings of the Second International Conference on Soil Mechanics and Foundation Engineering*, Rotterdam, vol. 6. 1948; 70–72.
5. Geddes JD. Stresses in foundation soils due to vertical subsurface loading. *Géotechnique* 1966; **16**(3):231–255.
6. Geddes JD. Tables for the calculation of stresses in a semi-infinite medium due to vertical subsurface loading. *Bulletin* 35, Department of Civil Engineering, University of Newcastle upon Tyne, 1966.
7. Wang CD. Displacement and stresses due to a vertical subsurface loading for a cross-anisotropic half-space. *Soils and Foundations* 2003; **43**(5):41–52.
8. Poulos HG. Settlement of single piles in nonhomogeneous soil. *Journal of Geotechnical Engineering Division* (ASCE) 1979; **105**(GT5):627–641.
9. Liao JJ, Wang CD. Elastic solutions for a transversely isotropic half-space subjected to a point load. *International Journal for Numerical and Analytical Methods in Geomechanics* 1998; **22**(6):425–447.
10. Wang CD, Tzeng CS, Pan E, Liao JJ. Displacements and stresses due to a vertical point load in an inhomogeneous transversely isotropic half-space. *International Journal of Rock Mechanics and Mining Sciences* 2003; **40**(5):667–685.
11. Longman IM. Tables for the rapid and accurate numerical evaluation of certain infinite integrals involving Bessel functions. *Proceedings of Cambridge Philosophical Society* 1956; **52**:166–180.
12. Watson GN. *A Treatise on the Theory of Bessel Functions*. Cambridge University Press: Cambridge, 1966.
13. Davis PJ, Rabinowitz P. *Methods of Numerical Integration* (2nd edn). Academic Press: New York, 1984.
14. Gazetas G. Stresses and displacements in cross-anisotropic soils. *Journal of Geotechnical Engineering Division* (ASCE) 1982; **108**(GT4):532–553.
15. Ward WH, Marsland A, Samuels SG. Properties of the London clay at the ashford common shaft. *Géotechnique* 1965; **15**(4):321–344.
16. Gibson RE. The analytical method in soil mechanics. *Géotechnique* 1974; **24**(2):115–140.
17. Lee KM, Rowe RK. Deformation caused by surface loading and tunneling: the role of elastic anisotropy. *Géotechnique* 1989; **39**(1):125–140.
18. Tarn JQ, Lu CC. Analysis of subsidence due to a point sink in an anisotropic porous elastic half space. *International Journal for Numerical and Analytical Methods in Geomechanics* 1991; **15**(8):573–592.

